

RUPTURE RISK PREDICTION OF INTRACRANIAL ANEURYSMS USING OPEN SOURCE CFD SOFTWARE

Oliveira, IL^{*}, Dias, ADSL^{*}, Militzer, J^{**}, Del Rio, ERV^{*}, Gasche, JL^{*} and Baccin, CE^{***}

^{*}São Paulo State University (Unesp) School of Engineering, Ilha Solteira, São Paulo, Brazil

^{**}Department of Mechanical Engineering, Dalhousie University, Halifax, Nova Scotia, Canada

^{***}Interventional Neuroradiology, Hospital Israelita Albert Einstein, São Paulo, Brazil.

ABSTRACT Computational Fluid Dynamics (CFD) is an important tool for simulating blood flow in intracranial aneurysms. The objective of this study is to help classify intracranial aneurysms based on data obtained from CFD simulations, so that the best treatment can be selected. We randomly selected 3 ruptured and 5 unruptured intracranial aneurysms with good quality CT angiogram (CTA). The open-source VMTK[®] (Vascular Modeling Toolkit) software was used to create surface models and CFD meshes. The open-source OpenFOAM[®] CFD solver was used to perform the CFD simulations and ParaView[®] was used for post-processing. Typical parameters associated with aneurysm rupture, such as wall shear stress (WSS), oscillatory shear index (OSI) and WSS gradient, were evaluated to determine if they may help predict aneurysm rupture probability. We have encountered regions where the WSS remained low during the entire cardiac cycle combined with high values of OSI and regions where the WSS remained high combined high WSS gradient. We associate these regions with high risk of rupture. This allowed us to predict, with a relatively high degree of certitude, the probability of rupture of a given aneurysm.

INTRODUCTION

Aneurysms are arterial lesions defined as thinned and dilated regions of the arterial wall. These abnormalities can arise in different areas of the human vascular system, more commonly found in the abdominal aorta and the arteries of the brain. Cases of intracranial aneurysms usually occur in the arterial bifurcations of the called circle of Willis (Figure 1). These aneurysms represent a high risk and can lead to neurological cerebral death with present mortality rates between 40 and 50 [e.g., Hop et al., 1997]. It is estimated also that 2-3% of the world population have intracranial aneurysms [e.g., Qureshi et al., 2007]. It is reported that 85% of cases of subarachnoid hemorrhage are caused by rupture of these aneurysms [e.g., van Gijn et al., 2007]. Hop et al. [1997] concluded that fatal cases of subarachnoid hemorrhage occurred from 32 to 67% of patients and about one third of those who survived showed permanent sequels.

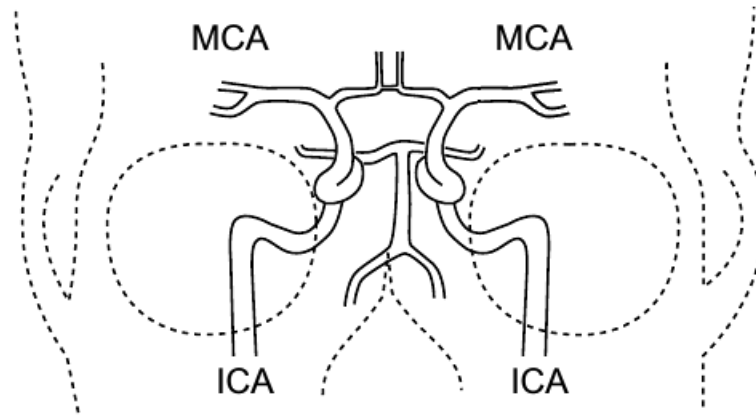


Figure 1. Schematic figure of the circle of Willis in the human brain (MCA: middle cerebral artery, ICA: internal carotid artery). [Torii et al., 2008]

Currently, there are no reliable experimental techniques for quantifying blood flow patterns in intracranial aneurysms. Measurements of hemodynamic parameters in live patients are becoming more achievable, but are still very difficult to perform. In general, experimental studies on intracranial aneurysms were performed using idealized geometries or induced aneurysms in animals [*e.g.*, Gonzalez et al., 1992; Nakatani et al., 1991; Satoh et al., 2003].

Computational Fluid Dynamics (CFD) techniques have been widely used to simulate flow problems in intracranial aneurysms [*e.g.*, Steinman et al., 2003; Bazilevs et al., 2009; Lu et al., 2011]. With the development of mapping techniques of the brain arteries (such as: Computational Tomography Angiography - CTA) numerical simulations with real geometries of aneurysms started to be performed, thereby increasing the reliability of the results.

Recent studies agree that effects of blood flow within the vessels (hemodynamic) are crucial in the development of aneurysms [*e.g.*, Penn et al., 2011]. Some of the hemodynamic parameters usually included in these studies are: the wall shear stress (WSS), the wall tension, the hydrostatic pressure and the transmural pressure. Among these parameters, the WSS seems to be the most important one [*e.g.*, Shojima et al., 2004; Sforza et al., 2009]. Also, Cebal and Cerrolaza [2003] studied the influence of the area and direction of the jet colliding in the aneurysm entrance and vortex formation inside the dome on the rupture of aneurysms.

The parameters leading to the formation, growth and rupture of intracranial aneurysms are still poorly understood. The purpose of this work is to test some cases of intracranial aneurysms using CFD to verify the influence of hemodynamic parameters in the rupture of aneurysms. The final objective of this type of work is to create a tool to be used in medical intervention decisions. To broaden the appeal and access to other researchers of the simulation methodology, we chose to use only open source software for creating surface contours from CTA, for meshing, for the CFD simulation and for post-processing. This will allow the community to make use of the tools we developed without being burdened by commercial software issues.

COMPUTATIONAL METHOD AND MATHEMATICAL MODELING

Problems found in Solid and Fluid Mechanics are governed by a set of partial differential equations, obtained from basic Physics conservation principles. Given the complex nature of the governing

mathematical equations it is impossible to obtain analytical solution to these equations. The problem is further complicated by the geometries involved. Thus, numerical techniques such as Finite Volume Method and Finite Element Method are required to solve them.

Computer packages are designed to numerically solve the governing equations using one of the above methods. In this work, we propose to use the OpenFOAM[®] (Open Field Operation and Manipulation) software to solve the numerical problem. This package is primarily a set of libraries written in C++ language that provides solvers to handle Continuum Mechanics problems.

The equations governing the blood flow through arteries are the conservation of mass and the linear momentum equation, Eqs. (1) and (2), for laminar flow and considering the blood as a Newtonian fluid with constant properties, namely: density $1,000\text{kg}/\text{m}^3$ and kinematic viscosity $3.3 \times 10^{-6}\text{m}^2/\text{s}$.

$$\nabla \cdot \mathbf{u} = 0 \quad (1)$$

$$\frac{\partial(\rho \mathbf{u})}{\partial t} + \nabla \cdot (\rho \mathbf{u} \mathbf{u}) = -\nabla p + \mu \nabla^2 \mathbf{u} \quad (2)$$

OpenFOAM[®] solves this system of partial differential equations using a cell-centered Finite Volume Method with a segregated approach, coupling the equations by using the Pressure Implicit with Splitting of Operators (PISO) algorithm [e.g., Moukalled et al., 2016].

The boundary conditions used were:

1. **Aneurysm Inlet:** transient mass flow condition as measured in the carotid artery [e.g., Womersley, 1955; Torii et al., 2008]. The velocity profile is shown in Figure 2, it also includes experimental data by Torii et al. [2008] which are compared with the data presented by Womersley [1955]. The inlet velocity of the flow was calculated from this data for each aneurysm geometry.

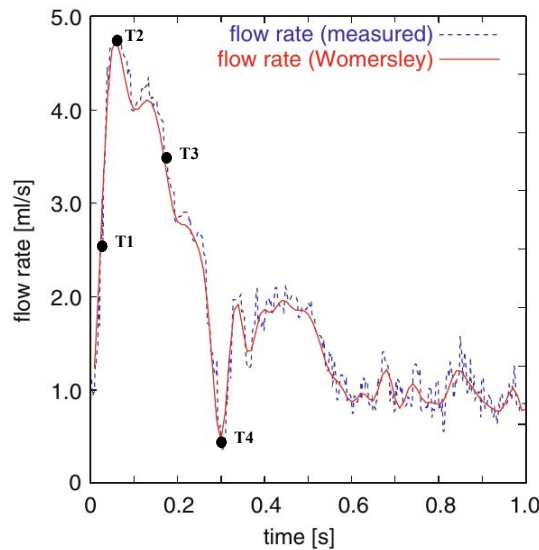


Figure 2. Transient blood velocity profile in the carotid artery used as inlet boundary condition in the simulations. [Torii et al., 2008]

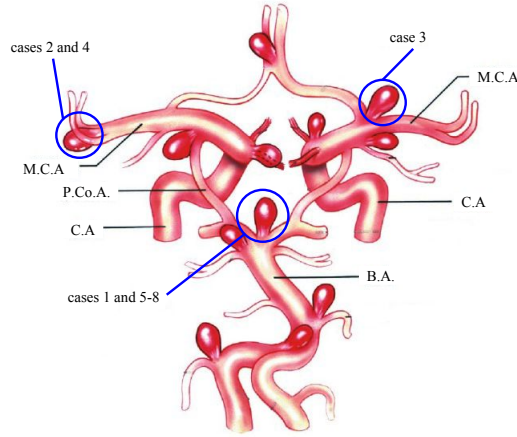


Figure 3. Aneurysms most common sites, and the locations of the ones in this work (MCA: middle cerebral artery, CA: internal carotid artery, BA: basilar artery and PCoA: posterior communicating artery). [Rhoton, 2002]

2. **Aneurysm Wall:** assumed rigid and no-slip condition.

3. **Aneurysm Outlet:** zero pressure.

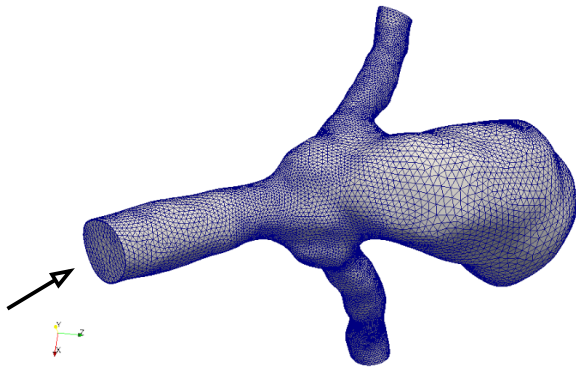
Eight random geometries of actual intracranial aneurysms were selected for the simulations. All the aneurysms are from brain arteries, and their location is shown in Figure 3. The geometric parameters of the aneurysms are shown in the Table 1: dome height, neck width and aspect ratio, here defined as the ratio between the dome height and neck width. The scans were taken from patients of the Victoria General Hospital in Halifax, Canada and Albert Einstein Hospital in São Paulo, Brazil, who provided the angiographic computed tomography (CTA) files. To ensure that the simulations were blind, we requested the doctors to omit the information as to which aneurysms were the ruptured or un-ruptured, so we could predict this characteristic based on our analysis of the simulation data.

The CTA files were imported into VMTK[®] - Vascular Modeling Toolkit graphics package. It is an open-source software providing a set of libraries and tools for 3D reconstruction, geometric analysis, mesh generation and surface data analysis for image-based modeling of blood flow in vessels. Figure 4 shows the meshes for each aneurysm model after treatment by VMTK[®] as used for the

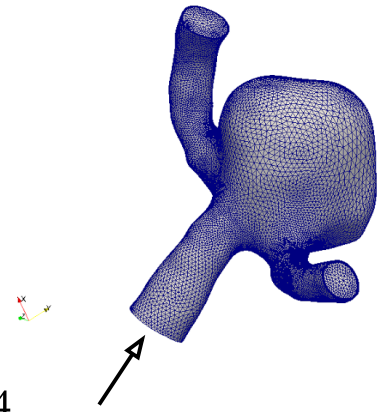
Table 1
Geometric parameters of the aneurysm.

	Neck (mm)	Dome height (mm)	Aspect Ratio
Case 1	4.1	8.2	2.0
Case 2	7.0	7.9	1.1
Case 3	4.2	5.7	1.3
Case 4	4.3	4.4	1.0
Case 5	4.3	4.8	1.1
Case 6	3.9	4.7	1.2
Case 7	3.5	4.6	1.3
Case 8	6.3	5.6	0.9

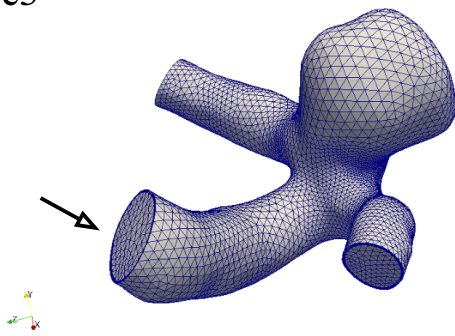
case1



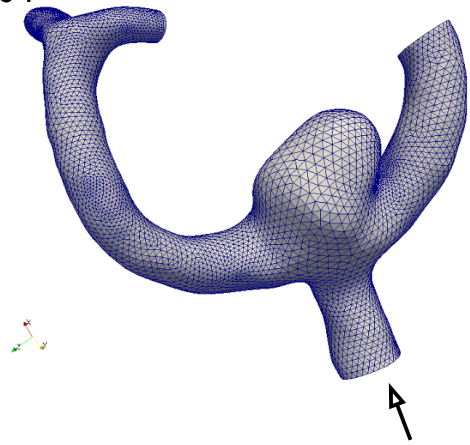
case2



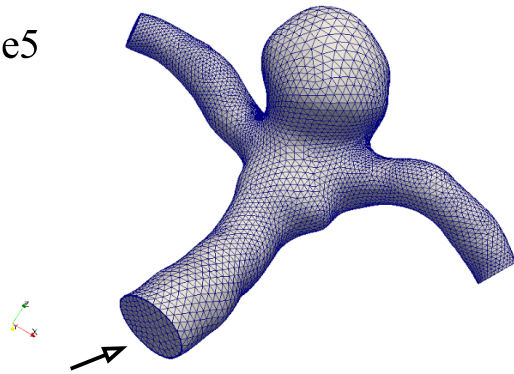
case3



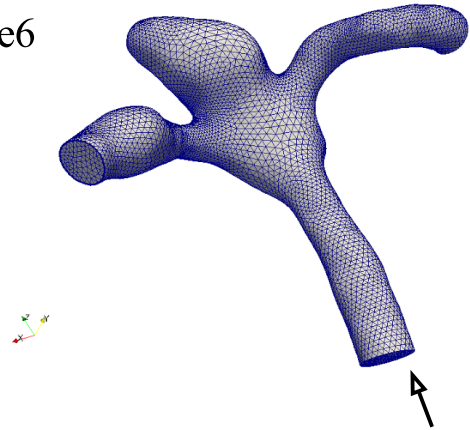
case4



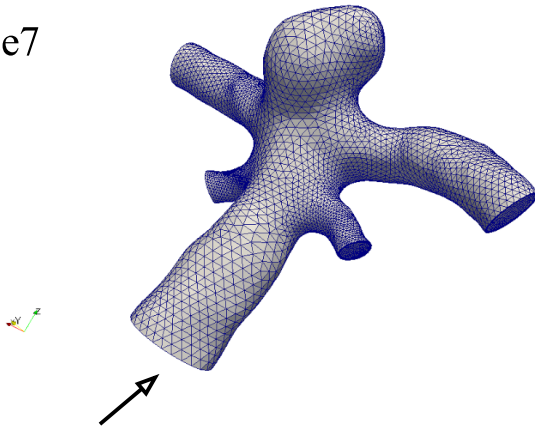
case5



case6



case7



case8

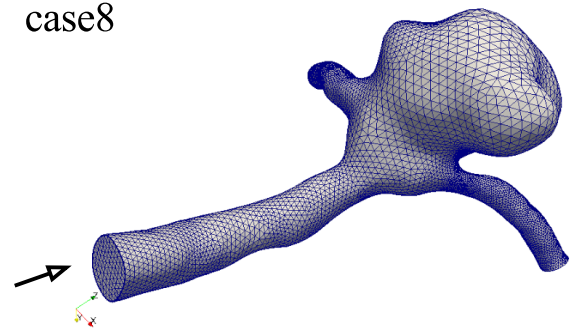


Figure 4. Meshes of the aneurysms models with smoothed surfaces after treatment in VMTK[®] with arrows indicating the inlet direction.

simulations. Note that the surfaces were smoothed using VMTK[®]. Figure 4 also shows, with an arrow, the flow inlet direction in each case.

Once the simulations were completed, we used the open-source software ParaView[®] for post-processing of the results. ParaView[®] has a large number of filters that allow obtaining and displaying various properties of the flow and its wall-fluid interface. We looked at the following variables:

- Velocity field to determine where the flow impinges the aneurysm;
- WSS and its gradient on the aneurysm internal surface;
- Oscillatory shear index (OSI), defined as:

$$OSI = \frac{1}{2} \left(1 - \frac{\left\| \int_0^T \mathbf{WSS} dt \right\|}{\int_0^T \|\mathbf{WSS}\| dt} \right) \quad (3)$$

where T is the cycle duration. This index measures the change of the WSS vector direction during the cardiac cycle.

RESULTS

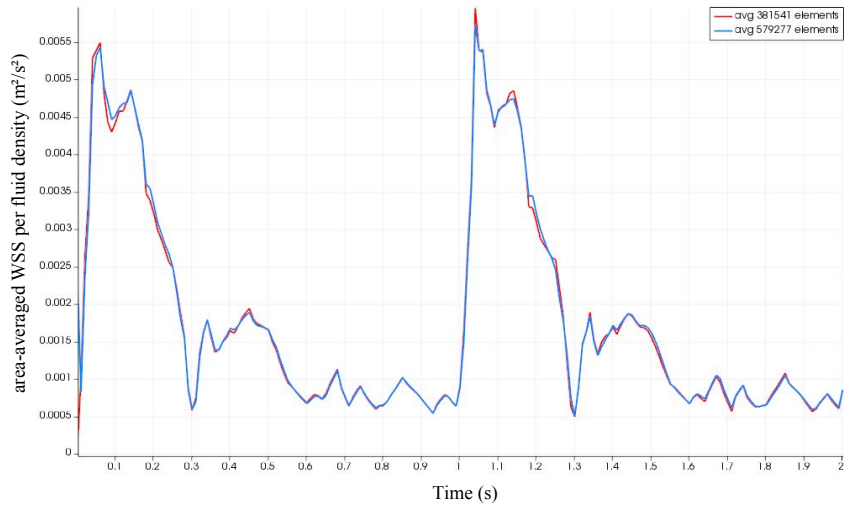
Numerical Accuracy We performed a grid refinement study using the area-averaged WSS (Eq. (4)) as parameter for comparing different meshes.

$$\overline{WSS}_S = \frac{1}{A_S} \left\| \int_S (\mathbf{WSS}) dS \right\| \quad (4)$$

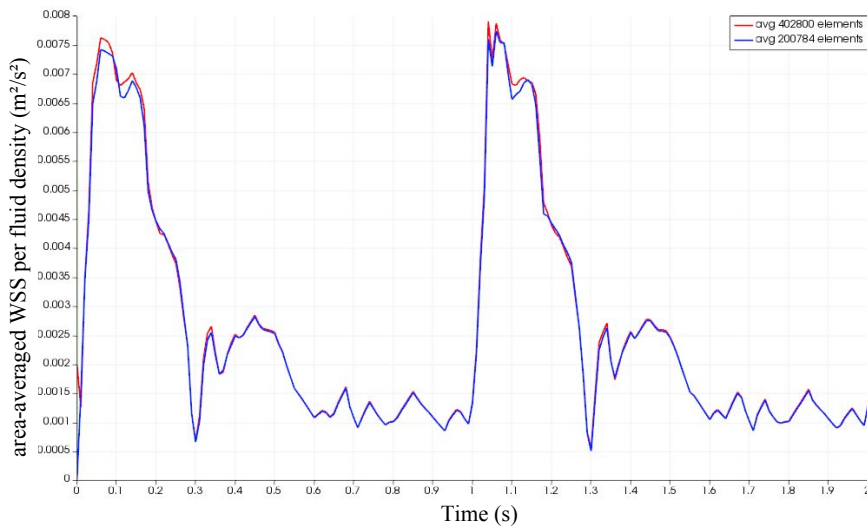
where A_S is the area of the surface S . The norm of the integral was calculated because WSS is a vector defined on the surface. Figures 5a, 6a and 5b present this quantity over time for the meshes of cases 2,3 and 4, respectively. These cases were chosen because they accurately represent the other cases since they share similar volume of the geometry and flow patterns. We followed the Richardson's method [e.g., Oberkampf and Trucano, 2002] for testing mesh independence. In essence we have doubled the number of elements of the mesh and compared the results. It is important to state that the meshes have boundary-layer refinement to improve solution accuracy near the wall.

In Figure 5a (case 2) we compare the results for area-averaged WSS for a grid with 381,541 elements with those of a grid with 579,277 elements. Similarly in Figure 6a (case 3) we consider three meshes with 114,148, 160,728 and 361,190 elements and in Figure 5b (case 4) we test meshes with 200,784 and 402,800 elements. In all three cases grid refinement did not significantly affect the results. Thus, we assume that the coarsest mesh is still adequate for the simulations. In all simulations we considered the solution to be converged when the normalized residuals were smaller than 1×10^{-6} for the pressure and 1×10^{-5} for the velocities.

To investigate the influence of the time step adopted, which in all simulations was $1 \times 10^{-4} s$, we ran case 3 with time steps of $0.5 \times 10^{-4} s$ and $1 \times 10^{-3} s$. Figure 6b shows the area-averaged WSS for case 3 with a mesh with 361,190 elements, for the different time-steps. It can be observed that the time step has no significant influence on the results, thus for all other cases we adopted a time step of $1 \times 10^{-4} s$.



(a)



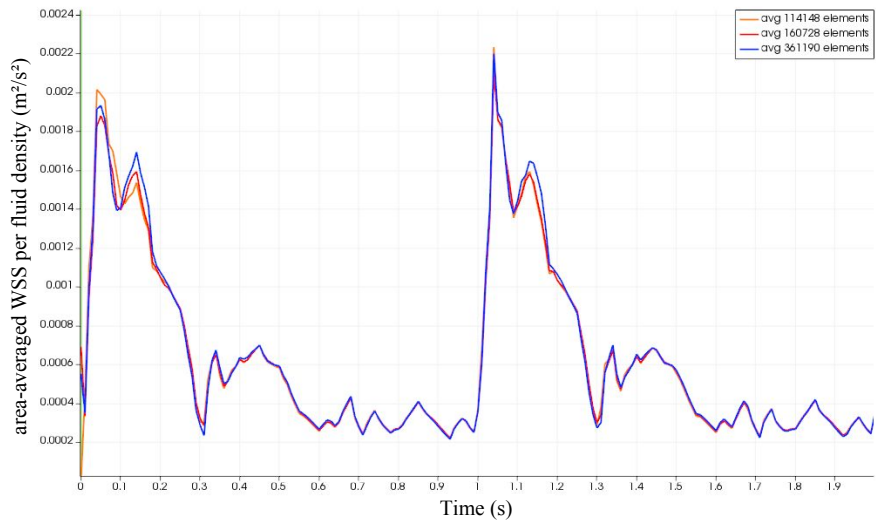
(b)

Figure 5. (a) Area-averaged WSS for case 2, indicating mesh independent solution; (b) Area-averaged WSS for case 4.

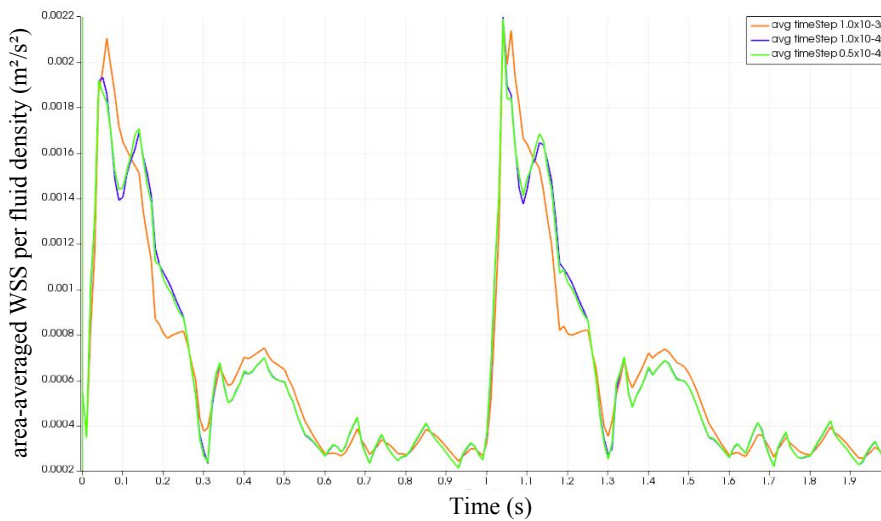
Simulations Results Figures 7 and 8 presents the results for the wall shear stress at four instants in the cardiac cycle. We analyzed the WSS values qualitatively, comparing its distribution throughout the surface of the aneurysm's dome. The instants considered are marked in Figure 2.

During the systolic peak (instant T2, Figure 2) we noticed a region of high WSS on the top of the aneurysms in cases 2, 4 and 6. Furthermore, it is possible to see regions with low levels of WSS in the entire cardiac cycle for cases 1, 6, 7 and 8 (Figures 7 and 8, points marked with an arrow) or during almost the entire cycle in cases 3 and 5 (Figures 7 and 8).

To determine the region of impingement of the flow in the aneurysms, Figure 9 shows sections of the eight aneurysms, not necessarily on the same axis. In cases 2, 6, and 8 the flow impinges the dome of the aneurysm while in cases 1, 4, 3, 5 and 7 the flow impinges the neck, causing a slow recirculation within the dome.



(a)



(b)

Figure 6. (a) Area-averaged WSS for case 3; (b) Area-averaged WSS for case 3 at different time-steps.

Figure 10 shows the WSS gradient for cases 2, 6 and 8. Where the impingement occurs we see that the WSS and its gradient reach high levels. Figure 11 shows the OSI distribution for each case. In cases 1, 7 and 8 we can verify the existence of OSI peaks at the aneurysm dome, while almost the whole artery is dominated by low levels of OSI.

CONCLUSIONS AND DISCUSSION

In their review paper, Meng et al. [2014] present different theories for the rupture of aneurysms, as presented in Figure 12. They concluded that both low and high WSS can cause the rupture of an aneurysm. The justification for this apparent contradiction is that low and high WSS act differently on the aneurysm: their presence leads to different biological events on the wall, which can lead to rupture.

According to Meng et al. [2014], the formation of the aneurysm is provoked by a high WSS value

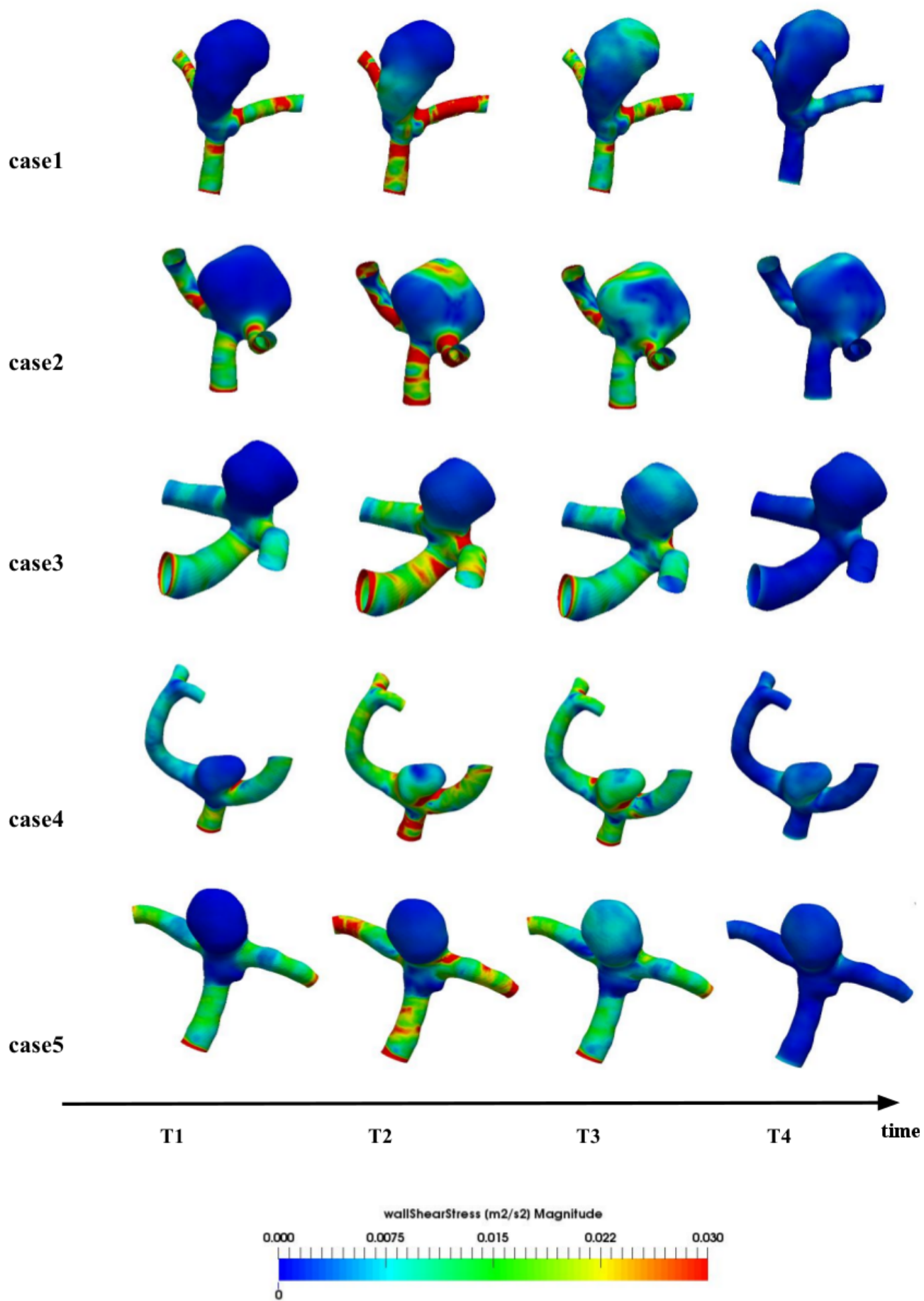


Figure 7. WSS for the aneurysms cases 1 to 5 at four instants of the cardiac cycle (the instants are marked in Figure 2 as T1, T2, T3 and T4).

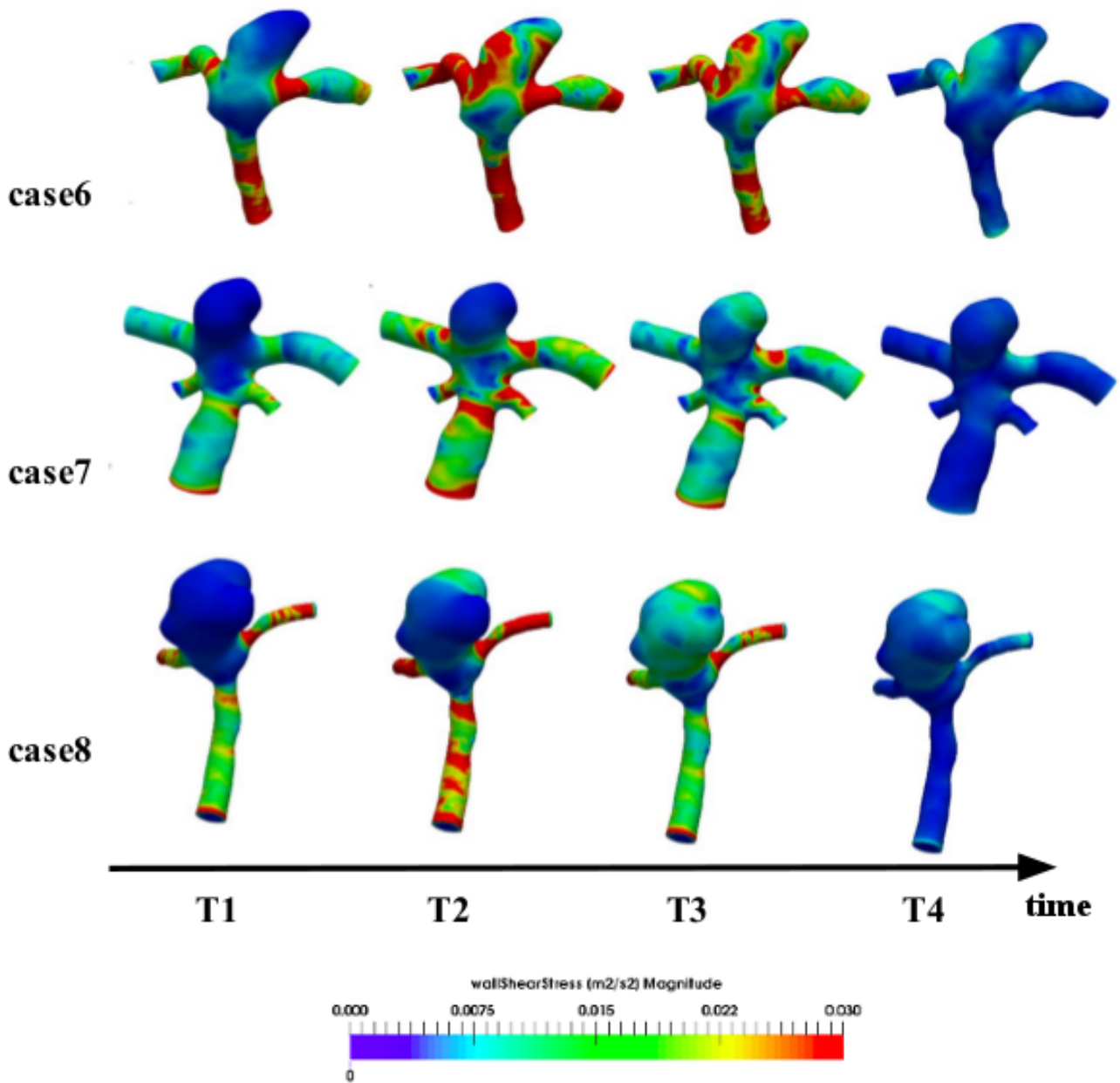


Figure 8. WSS for the aneurysms cases 6, 7 and 8 at four instants of the cardiac cycle (the instants are marked in Figure 2 as T1, T2, T3 and T4).

combined with a positive gradient of the WSS, however there are two different mechanisms responsible for the growth according to the type of flow within the aneurysm and the level of WSS:

1. *Flow impinging at aneurysm dome*: when combined with high WSS and a positive WSS gradient, can cause the formation of a bleb, with weakened walls that can lead to the rupture of the aneurysm.
2. *Recirculation combined with low WSS and high oscillatory shear index (OSI)*: can lead to the formation of thrombus, changing the shape of the aneurysm and eventually causing its rupture.

Other authors [e.g., Lu et al., 2011; Cebal and Cerrolaza, 2003; Shojima et al., 2004] associate ruptured aneurysms exclusively with low WSS. Wall shear stress areas are considered low when their values are smaller than $0.015 \text{ m}^2/\text{s}^2$ (per unit of fluid density) [e.g., Lu et al., 2011]. We can see in

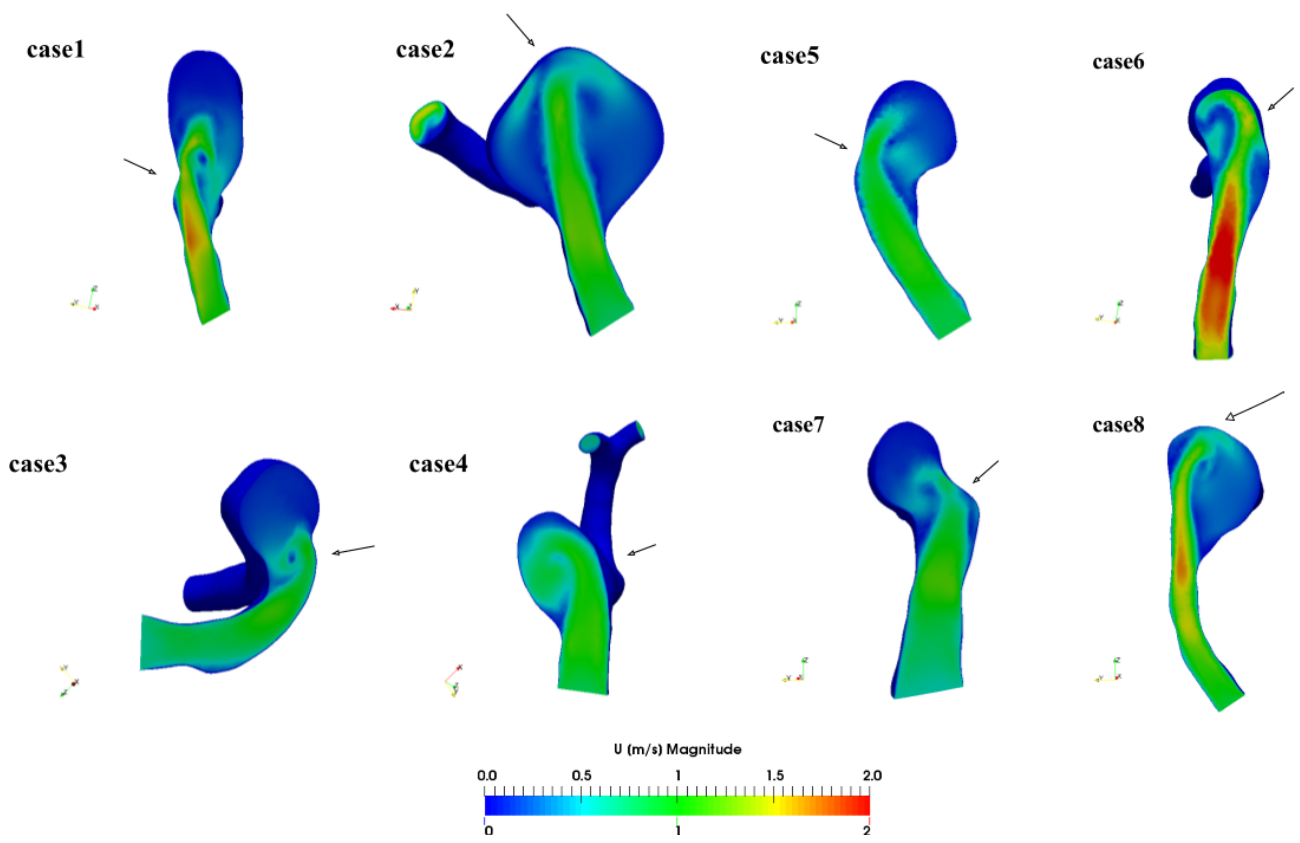


Figure 9. Velocity field for the aneurysm flow in the systolic peak, showing the impingement region.

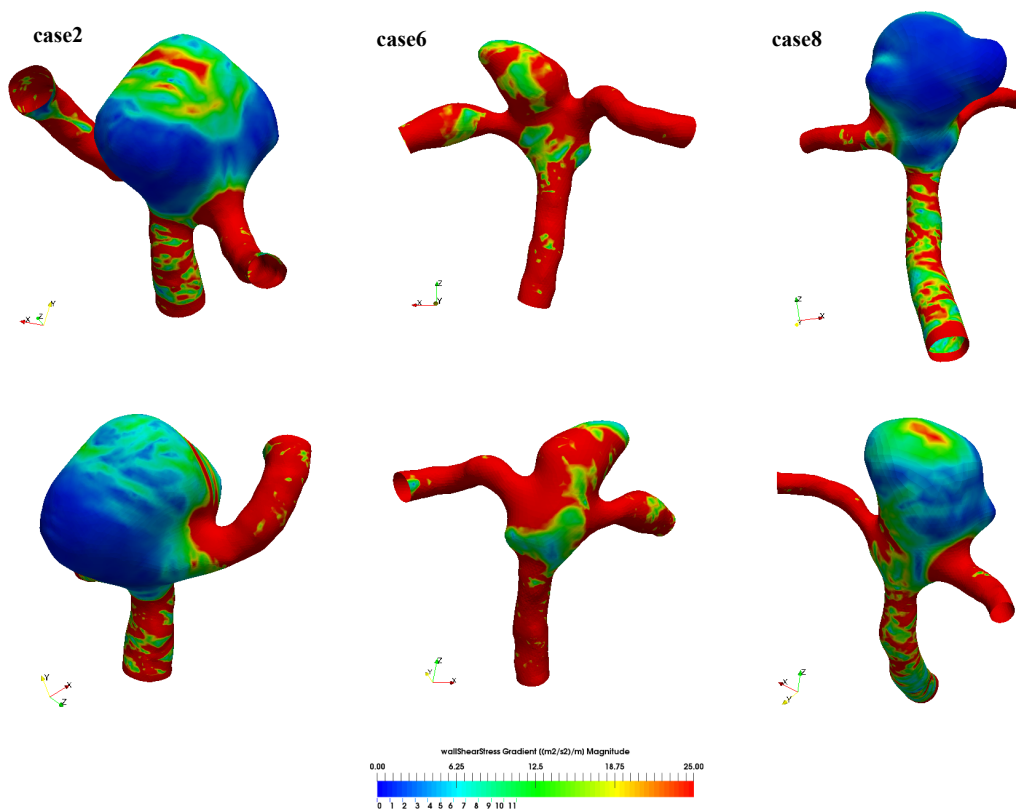


Figure 10. Front and back views showing the WSS gradient on the surface of cases 2, 6 and 8, where high levels occur due to the impingement flow at the aneurysm dome

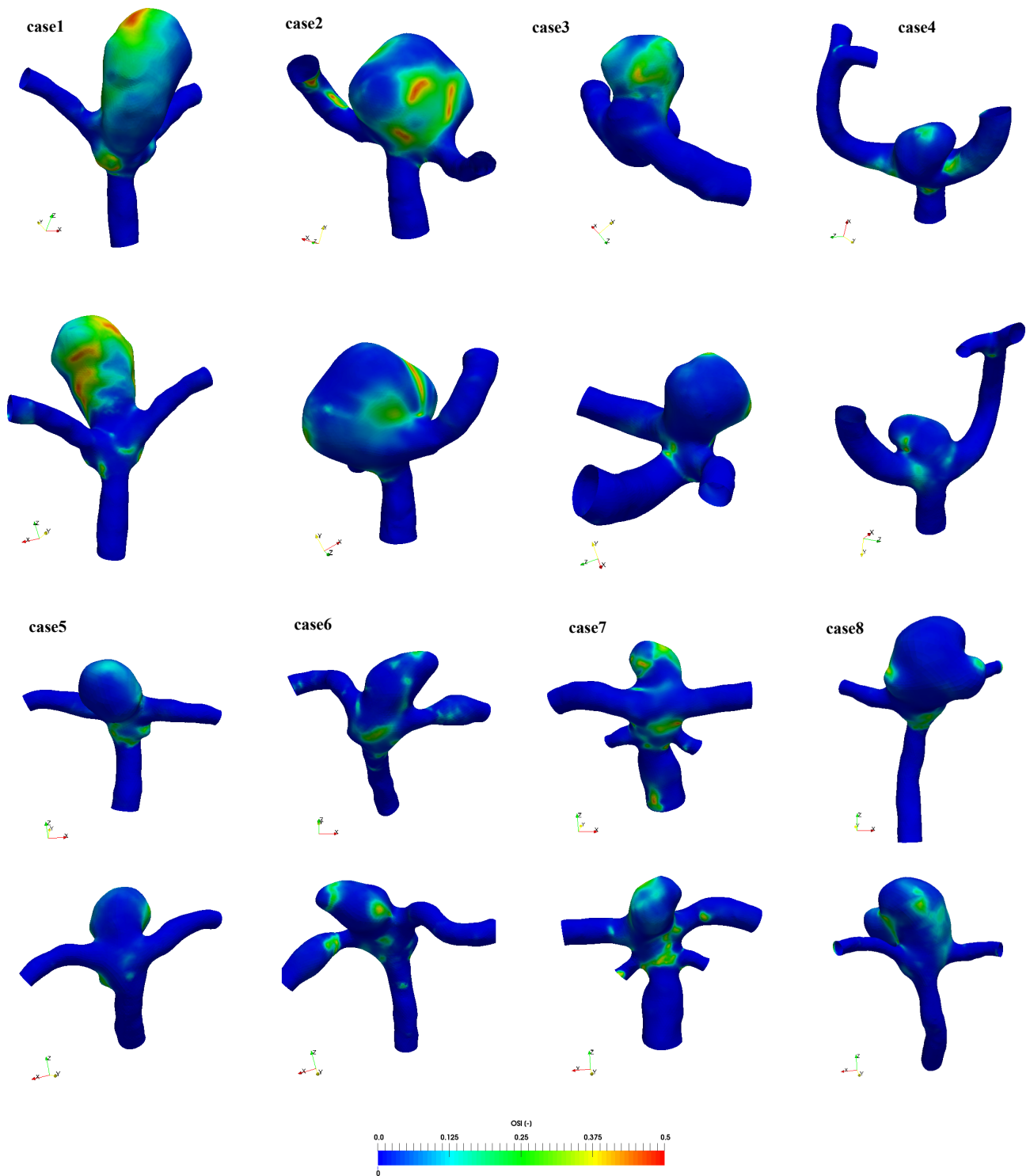


Figure 11. Front and back views showing the OSI fields.

the results of cases 1, 7 and 8 (Figures 7 and 8), clearly defined regions of low WSS throughout the cardiac cycle (Figures 7 and 8, positions marked with an arrow).

Cases 1, 7 and 8 also show peaks of OSI on the aneurysm dome (Figure 11). More precisely, these regions occur where the surface is very irregular. Thus, we arrive at the conclusion that the aneurysms having regions where low levels of WSS occur during the entire cardiac cycle and with high OSI are likely ruptured aneurysms.

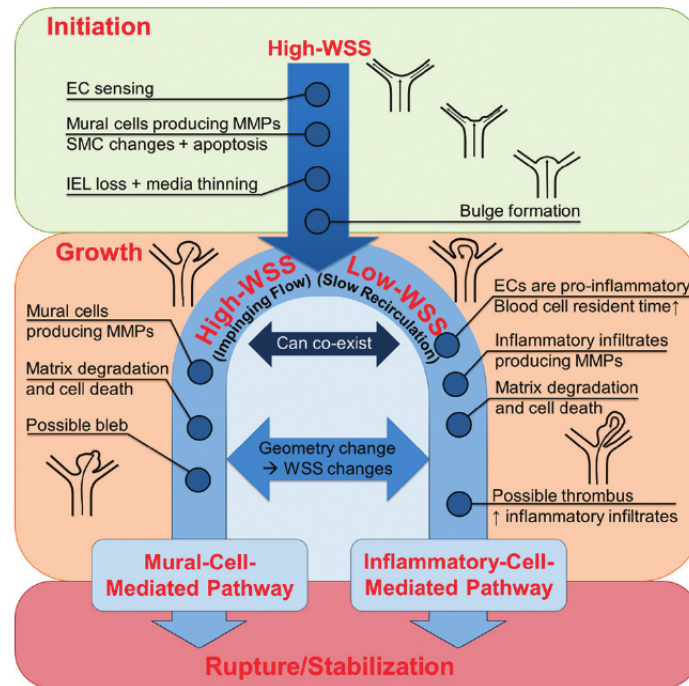


Figure 12. High and low flow effects on intracranial aneurysm rupture. [Meng et al., 2014]

Aneurysms 2, 4 and 6 have high levels of WSS at the dome because of the location of the flow impingement within the aneurysm, but the levels of WSS gradient, in these locations, are high only for cases 2 and 6 (Figure 10) and thus according to Meng et al. [2014] have a higher risk of rupture.

Based on these observations combined with those of Lu et al. [2011] on high WSS, we propose an aneurysm rupture probability scale (low, high and very high). The criteria are summarized below.

- Aneurysms with impinging flow combined with:
 - High WSS and positive WSS gradient → high;
 - High WSS and negative WSS gradient → low;
- Aneurysms with recirculation presenting:
 - low WSS and high OSI → high;
 - low WSS and low OSI → low;
- Aneurysms with recirculation and impinging flow → very high;

The size of the aneurysm is also an important factor. According to Qureshi et al. [2007], small aneurysms (height smaller than 7mm), have a 0% rupture rate. Thus if the aneurysm is large (> 7mm) the level goes up a notch. Table 2 summarizes these ideas.

We reported that we considered cases 1, 2, 6, 7 and 8 as possibly ruptured to the doctors who had provided the CT-Scans. They confirmed our conclusion that indeed cases 6, 7 and 8 were ruptured aneurysms. These results confirm that hemodynamic variables can be used as indicators of the possibility of rupture of an aneurysm. Cases 1 and 2 were unruptured. In case 2 this is probably because it has received a stent. But it is very likely that these cases would eventually develop irregularities in both the aneurysm size and shape, which consequently, could lead to their rupture. Hence, it would be prudent to continue to monitor these cases in order to verify our suspicions.

Table 2
Summary of results.

	Flow type	WSS level	OSI	WSS gradient	Height (mm)	Our probability of rupture	Observations
Case 1	Recirculation	Low	High	Low	8.2	Very high ^b	Unruptured
Case 2	Impingement ^a	High	High	High	7.9	Very high ^b	Unruptured (treated)
Case 3	Recirculation	Low	High	Low	5.7	High ^c	Unruptured (treated)
Case 4	Impingement	Low	Low	Low	4.4	Low	Unruptured (treated)
Case 5	Recirculation	Low	Low	Low	4.8	Low	Unruptured
Case 6	Impingement ^a	High	High	High	4.7	Very high	Ruptured
Case 7	Recirculation	Low	High	Low	4.6	High	Ruptured
Case 8	Recirculation ^a	Low	High	High	5.6	Very high	Ruptured

^a These cases actually show both an impingement on the aneurysm wall and recirculating flow due to some thrombus in its surface, each region with the conditions of WSS and OSI that may lead to rupture, according to Meng et al. [2014]. Since they present both critical conditions, we propose a very high risk of rupture.

^b The flow type, WSS level, OSI and WSS gradient combinations according to Meng et al. [2014] for these cases could lead to rupture. Since these aneurysms are very large, we propose a very high risk of rupture.

^c The risk is high, but since they are small we would recommend their monitoring for possible thrombus formation.

Our results have confirmed, at some level, that WWS and some characteristics of the flow, like impingement direction, WSS gradients and OSI, can be related to aneurysm rupture events. Further simulations with new aneurysms, ruptured or not, will be performed to increase the data base to verify agreement with our conclusions. In any case, CFD simulations have proved to be a valuable tool in the analysis of biological flows such as the ones occurring in aneurysms.

ACKNOWLEDGEMENT

The authors would like to thank Dr. J.J. Shankar (Dalhousie Medical School, Department of Radiology, Halifax, Canada) for providing the CT scan of cases 1, 5, 6, 7 and 8 and for engaging in valuable discussions. This research was partly supported by resources supplied by the Center for Scientific Computing (NCC/GridUNESP) of the São Paulo State University (UNESP) and Acenet (Dalhousie University).

REFERENCES

- Bazilevs, Y., Hsu, M. C., Benson, D. J., Sankaran, S. and Marsden, A. L. [2009], ‘Computational fluid-structure interaction: Methods and application to a total cavopulmonary connection’, *Computational Mechanics* **45**(1), 77–89.
- Cebral, J. R. and Cerrolaza, M. [2003], Computational Analysis of Blood Flow Dynamics in Cerebral Aneurysms from CTA and 3D Rotational Angiography Image Data, in ‘International Congress on Computational Bioengineering’.

- Gonzalez, C. F., Cho, Y. I., Ortega, H. V. and Moret, J. [1992], 'Intracranial aneurysms: Flow analysis of their origin and progression', *American Journal of Neuroradiology* **13**(1), 181–188.
- Hop, J. W., Rinkel, G. J., Algra, A. and van Gijn, J. [1997], 'Case-Fatality Rates and Functional Outcome After Subarachnoid Hemorrhage : A Systematic Review', *Stroke* **28**(3), 660–664.
URL: <http://stroke.ahajournals.org/cgi/content/long/28/3/660>
- Lu, G., Huang, L., Zhang, X. L., Wang, S. Z., Hong, Y., Hu, Z. and Geng, D. Y. [2011], 'Influence of hemodynamic factors on rupture of intracranial aneurysms: Patient-specific 3D mirror aneurysms model computational fluid dynamics simulation', *American Journal of Neuroradiology* **32**(7), 1255–1261.
- Meng, H., Tutino, V. M., Xiang, J. and Siddiqui, A. [2014], 'High WSS or Low WSS? Complex interactions of hemodynamics with intracranial aneurysm initiation, growth, and rupture: Toward a unifying hypothesis', *American Journal of Neuroradiology* **35**(7), 1254–1262.
- Moukalled, F., Mangani, L. and Darwish, M. [2016], *The Finite Volume Method in Computational Fluid Dynamics*, Vol. 113, Springer.
URL: <http://www.scopus.com/inward/record.url?eid=2-s2.0-84939129919&partnerID=tZOtx3y1>
- Nakatani, H., Hashimoto, N., Kang, Y., Yamazoe, N., Kikuchi, H., Yamaguchi, S. and Niimi, H. [1991], 'Cerebral blood flow patterns at major vessel bifurcations and aneurysms in rats.', *Journal of neurosurgery* **74**(2), 258–62.
URL: <http://www.ncbi.nlm.nih.gov/pubmed/1988596>
- Oberkampf, W. L. and Trucano, T. G. [2002], 'Verification and Validation in Computational Fluid Dynamics 1', *Progress in Aerospace Sciences* **38**(March 2002), 210–270.
- Penn, D. L., Komotar, R. J. and Sander Connolly, E. [2011], 'Hemodynamic mechanisms underlying cerebral aneurysm pathogenesis', *Journal of Clinical Neuroscience* **18**(11), 1435–1438.
URL: <http://dx.doi.org/10.1016/j.jocn.2011.05.001>
- Qureshi, A. I., Janardhan, V., Hanel, R. A. and Lanzino, G. [2007], 'Comparison of endovascular and surgical treatments for intracranial aneurysms: an evidence-based review', *Lancet Neurology* **6**(9), 816–825.
- Rhoton, A. L. [2002], Aneurysms, in 'Neurosurgery', Vol. 51, pp. 121–158.
- Satoh, T., Onoda, K. and Tsuchimoto, S. [2003], 'Visualization of intraaneurysmal flow patterns with transluminal flow images of 3D MR angiograms in conjunction with aneurysmal configurations', *American Journal of Neuroradiology* **24**(7), 1436–1445.
- Sforza, D. M., Putman, C. M. and Cebal, J. R. [2009], 'Hemodynamics of Cerebral Aneurysms', *Annual Review of Fluid Mechanics* **41**, 91–107.
- Shojima, M., Oshima, M., Takagi, K., Torii, R., Hayakawa, M., Katada, K., Morita, A. and Kirino, T. [2004], 'Magnitude and Role of Wall Shear Stress on Cerebral Aneurysm: Computational Fluid Dynamic Study of 20 Middle Cerebral Artery Aneurysms', *Stroke* **35**(11), 2500–2505.
- Steinman, D. A., Milner, J. S., Norley, C. J., Lownie, S. P. and Holdsworth, D. W. [2003], 'Image-based computational simulation of flow dynamics in a giant intracranial aneurysm.', *AJNR. American journal of neuroradiology* **24**(4), 559–66.
URL: <http://www.ajnr.org/content/24/4/559.abstract>

- Torii, R., Oshima, M., Kobayashi, T., Takagi, K. and Tezduyar, T. E. [2008], 'Fluid-structure interaction modeling of a patient-specific cerebral aneurysm: Influence of structural modeling', *Computational Mechanics* **43**(1), 151–159.
- van Gijn, J., Kerr, R. S. and Rinkel, G. J. E. [2007], 'Subarachnoid haemorrhage.', *Lancet* **369**(9558), 306–318.
- Womersley, J. R. [1955], 'Method for the Calculation of the Velocity, Rate of Flow and Viscous Drag in Arteries When the Pressure Gradient is Known', *Journal of Physiology* **127**(2), 553–563.